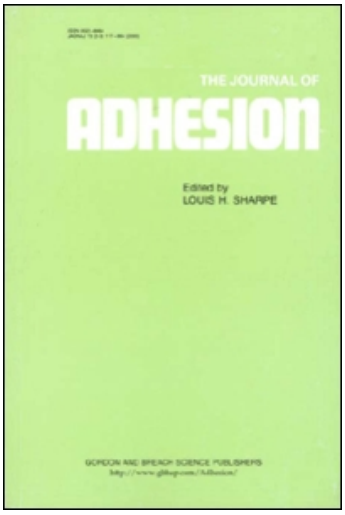

The Journal of Adhesion
Publication details, including instructions for authors and subscription information:
http://www.informaworld.com/smpp/title~content=t713453635

Surface Energy Analysis of Treated Graphite Fibers

D. H. Kaelble[a]; P. J. Dynes[a]; L. Maus[b]
[a] Science Center, Rockwell International, Thousand Oaks, California, U.S.A. [b] Tulsa Division, Rockwell International, Tulsa, Oklahoma, U.S.A.

To cite this Article Kaelble, D. H. , Dynes, P. J. and Maus, L.(1974) 'Surface Energy Analysis of Treated Graphite Fibers', The Journal of Adhesion, 6: 3, 239 — 258
To link to this Article: DOI: 10.1080/00218467408075029
URL: http://dx.doi.org/10.1080/00218467408075029

J. Adhesion, 1974, Vol. 6, pp. 239–258

Printed in Scotland

Surface Energy Analysis of Treated Graphite Fibers

D. H. KAELBLE, P. J. DYNES

Science Center, Rockwell International, Thousand Oaks, California 91360, U.S.A.

and

L. MAUS

Tulsa Division, Rockwell International, Tulsa, Oklahoma 74151, U.S.A.

(*Received September 28, 1973*)

Wettability measurements and surface energy analysis are applied to isolate the (London-*d*) and (Keesom-*p*) polar contributions to solid–vapor surface tension $\gamma_{SV} = \gamma^d_{SV} + \gamma^p_{SV}$ of surface treated graphite fibers. Surface treatments include metal coatings with Al, Cu, and Ni, chemically reducing heat treatments in H_2 and vacuum, and films of highly chlorinated polymers such as polyhexachlorobutadiene and polychloral. This study shows that the highly polar surface properties $\gamma^p_{SV}/\gamma_{SV} \simeq \gamma^d_{SV}/\gamma_{SV} \simeq 0.50$ of commercial graphite fibers can be modified by surface treatment to display dominant dispersion character with $\gamma^d_{SV}/\gamma_{SV} \simeq 0.79$ to 0.92 without substantial reduction in total surface energy γ_{SV}. For adsorption bonded fiber/matrix interfaces a new method of mapping the surface energy effects of an immersion phase upon the Griffith fracture energy γ_G is applied to define criteria for strong interfacial bonding under both air and water immersion.

INTRODUCTION

This study forms part of a more general program addressed to developing a better understanding of the relationships between mechanisms of interfacial bonding and environmental stability in polymer matrix composites.[1-3] Recent studies have shown that exposure of graphite reinforced epoxy or polyester matrix composites to water immersion or water vapor at elevated temperature produces a serious deterioration in interlaminar shear strength and fracture toughness.[3, 4] One approach to the correction of this moisture sensitivity has been suggested by Kaelble[3] based upon a modified Griffith–Irwin model which redefines the reversible Griffith fracture energy γ_G in terms of the (London-*d*) dispersion γ^d and (Keesom-*p*) polar contributions to the

nominal surface energies of the fiber, matrix, and immersion phase. Such a model predicts that the fracture energy γ_G under water immersion should be approximately equal to γ_G in air when both the fiber and matrix have low polar ($\gamma^p_{SV} \leqslant 1.0$ dyn/cm) and high dispersion ($\gamma^d_{SV} \geqslant 36.0$ dyn/cm) solid–vapor surface energy components. In the present investigation surface treatments for graphite fibers will be described which result in a decreased polar and increased dispersion surface energy as determined by wettability measurements and surface energy analysis.

MATERIALS AND METHODS

Fibers included in this study include Hercules HT–S® and HM–S® graphite fibers which were characterized and treated in the as-received condition. Thornel 400® produced by Union Carbide Corp. was treated to remove

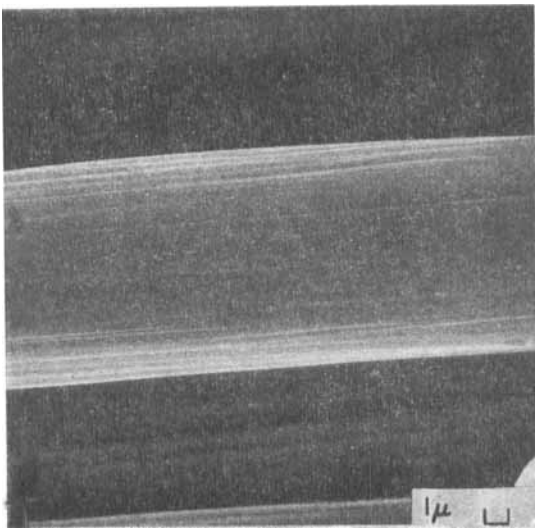

FIGURE 1 SEM view (4000×) of virgin Hercules HT–S® graphite fiber showing relatively smooth surface with longitudinal striations characteristic of polyacrylonitrile (PAM) precursor.

a polyvinyl alcohol size prior to surface characterization and surface treatment. These fibers display the relatively smooth surface and circular cross-section typical of graphitized polyacrylonitrile (PAN). A scanning electron micrograph (SEM) view of virgin HT–S fiber is shown in Figure 1 and typifies the topology of untreated fibers examined in this investigation.

Aluminum coated graphite fibers were prepared by the Dow Chemical Company using a patented method[5] which consists of the following seven steps:

1) Dry fiber for 48 hour in vacuum oven at 120°C.

2) Transfer to nitrogen atmosphere dry box without moisture pickup (all subsequent operations are performed in this dry box atmosphere).

3) Catalyze fiber surface in $TiCl_4$ vapors for 1.0 minute.

4) Allow to dry in atmosphere of box.

5) Dip fibers into 0.5 molar diethyl ether solution of aluminum hydride etherate.

6) Remove excess liquid.

7) Heat for 1.0 minute at 150°C to produce Al coating.

The SEM view of an aluminum coated Thornel 400® fiber prepared as described above is shown in Figure 2. It is evident that the Al film covers the sharp striations of the virgin fiber surface (see Figure 1) and displays some nodular structure due to selective film growth rates.

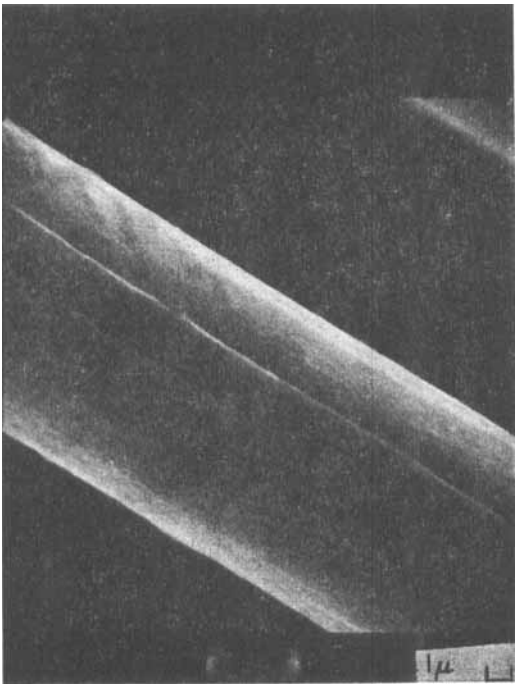

FIGURE 2 SEM view (4000×) of aluminum coated Thornel 400® fiber.

Copper coated Thornel 400® was prepared in the following manner:[6]

1) Graphite yarn was first cleaned in a chromic acid solution to remove residual PVA size.

2) A thin copper coating was applied using an electrodeless method based on reduction of Fehling's solution.

3) The fiber was then "sensitized" in stannous chloride and "activated" in palladium chloride.

4) Copper is then electrolytically plated to the desired thickness in an acidic copper sulphate bath.

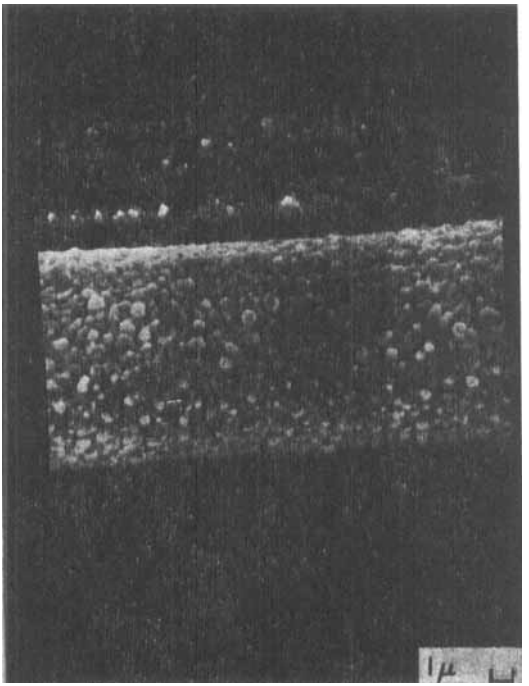

FIGURE 3 SEM view (3500×) of copper coated Thornel 400® fiber ($3.0 \cdot 10^{-5}$ inch thick coating).

The SEM view of the electroplated copper film formed on Thornel 400® fiber shown in Figure 3 displays a complete coverage of the original surface detail of the virgin fiber (see Figure 1) and development of a highly nodular surface topology.

Nickel coated fibers of Hercules HT-S® were prepared using a proprietary Rockwell International Corporation surface treatment. The SEM view of

Figure 4 shows a typical fiber surface prepared by this method. It is evident that the coating is extremely thin since the nickel coated fiber displays the striated topology characteristic of the virgin fiber (see Figure 1). It is also evident in Figure 4 that only isolated metal nodules protrude through the relatively uniform nickel coating.

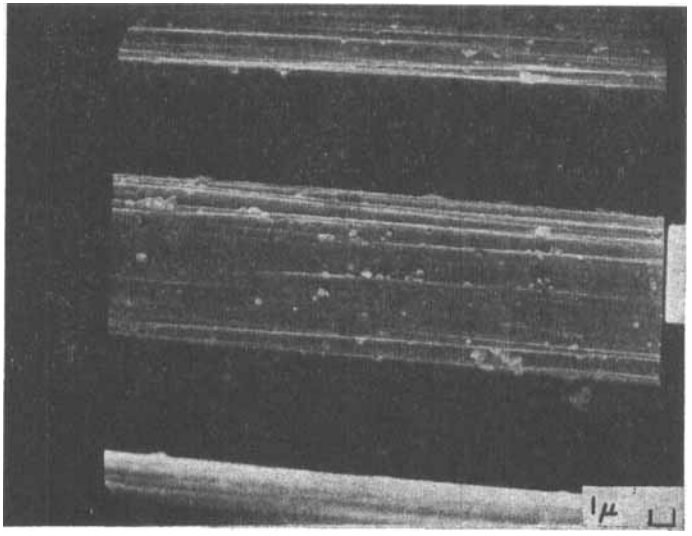

FIGURE 4 SEM view (4000×) of nickel coated Hercules HT-S® fiber (Rockwell treatment #2).

An additional sample of nickel coated Hercules HT-S® graphite fiber was commercially obtained from the Shipley Company. The SEM view of this fiber surface shown in Figure 5 reveals a thick nickel coating containing isolated spherical cap nodules.

Two thermal treatments were applied to chemically reduce polar surface functionality on Hercules HT-S® graphite fiber. Hydrogen treated HT-S® fiber was prepared by heating a section of yarn at 1000°C for 1.0 hour in a flowing 50/50 mixture of argon and hydrogen for 1 hour. Vacuum heat treated HT-S® fiber was obtained by heating a yarn sample at 1000°C for 1 hour in a 10^{-6} torr vacuum.

Coatings or films of polyhexachlorobutadiene were prepared using the surface photo-polymerization method described by Wright[7] and Kunz and coworkers.[8] Using this procedure Thornel 400® graphite fiber or clean glass microscope slides were evacuated to a pressure of 10^{-4} torr in a quartz tube. With vacuum to the system closed off, hexachlorobutadiene vapor is allowed to enter the quartz tube from a liquid supply maintained at 18°C. The vapor

pressure of hexachlorobutadiene at this temperature is ~135 microns.[8] An ultraviolet pen lamp is then applied to irradiate the fiber or glass slide surfaces for a period of 8 hours. The quartz tube was then evacuated to 10^{-4} torr and the samples were reirradiated for 2 hours in vacuum.

Samples of polychloral $\{HC(CCl_3)O\}_n$ were obtained from the du Pont Company as a 2.5 mm thick sheet of a 95/5 mole ratio copolymer of chloral with *p*-chlorophenyl isocyanate. These films were evaluated for comparative surface energy properties with the polyhexachlorobutadiene coatings and films.

FIGURE 5 SEM view (4000×) of nickel coated Hercules HT-S® (proprietary Shipley Company treatment).

Advancing contact angles between test liquids and single fibers were measured using the automatic micro-Wilhelmy plate method described by Neumann and Tanner[9] and Mozzo and Chabord.[10] In this method the contact force ΔM (gm) between a fiber of circumference C and a liquid of surface tension γ_{LV} is described by the following relation:

$$\Delta M = \frac{\gamma_{LV} C \cos\theta}{g} \tag{1}$$

where θ is the advancing liquid–solid contact angle and $g = 980.6$ dyn/gm. Wetting liquids which form zero contact angle on the fiber surface provide $\cos\theta = 1.0$ in Eq. (1) and permit direct calculation of fiber circumference. The force ΔM is measured by a recording CAHN electrobalance whose sensitivity is 0.2 μgm. Fiber contact angle measurements were conducted at 22.0 ± 1.0°C and $50 \pm 5\%$ R.H. in ambient laboratory environment. The *advancing* liquid–solid angles on film samples were measured at 20°C in the B–100 environmental chamber of the NRL goniometer, Model A–100 (Rame–Hart, Inc.).

The test liquids utilized in these wettability measurements are listed in Table I in descending order of surface tension γ_{LV} values. The platinum–iridium Wilhelmy plate technique was applied to measure the surface tension of these liquids. Agreement between experimental and literature values of liquid surface tension, within ± 0.5 dyn/cm, is taken as evidence of liquid purity and literature values [11, 12] for γ_{LV}^d and γ_{LV}^p are applied in the surface energy analysis. The conventional relations for describing the (London-*d*) dispersion and (Keesom-*p*) polar interactions between liquids and solids are stated as follows:[1, 3, 13]

$$\gamma_{LV} = \gamma_{LV}^d + \gamma_{LV}^p = \alpha_L^2 + \beta_L^2 \tag{2}$$

$$\gamma_{SV} = \gamma_{SV}^d + \gamma_{SV}^p = \alpha_S^2 + \beta_S^2 \tag{3}$$

$$\gamma_{SV} = \gamma_{S^\circ} - \pi_e \tag{4}$$

$$W_a = \gamma_{LV}(1 + \cos\theta) \leqslant 2\gamma_{LV} \tag{5}$$

$$W_a = 2[\alpha_L\alpha_S + \beta_L\beta_S] \tag{6}$$

$$\frac{W_a}{2\alpha_L} = \alpha_S + \beta_S(\beta_L/\alpha_L). \tag{7}$$

The symbols for Eq. (2) through Eq. (7) are defined in Table II. When reference is made to high energy solids such as glass, ceramics, metals, and metal oxides, a common confusion exists by assuming $\gamma_{SV} \simeq \gamma_{S^\circ}$ where γ_{S° is the surface tension of the virgin solid in vacuum. When such surfaces are exposed to ambient atmosphere, studies show that π_e is nearly equal to γ_{S° which points out that γ_{SV} is primarily influenced by the chemical constitution of the adsorption layer on the solid surface.[11, 13] In contrast, organic polymer surfaces generally display $\pi_e \simeq 0$ so that $\gamma_{SV} \simeq \gamma_{S^\circ}$ and the determined values of γ_{SV} provided by Eq. (2) through Eq. (7) from measurements at ambient conditions correlate closely with the virgin surface in vacuum.

The determination of γ_{SV} is relevant to interfacial adhesion studies since interfacial bonds are normally formed or broken under ambient atmospheric conditions. The major emphasis in surface energy analysis is to isolate by calculation the values of $\gamma_{SV}^d = \alpha_S^2$ and $\gamma_{SV}^p = \beta_S^2$ based upon wettability

measurements with liquids of known $\gamma_{LV}^d = \alpha_L^2$ and $\gamma_{LV}^p = \beta_L^2$. Nominal values for work of adhesion, as defined by Eq. (5) for $\theta > 0$ may be analyzed by either Eq. (6) or Eq. (7). From Eq. (7) we recognize a simple method of graphical analysis wherein a plot of $W_a/2\alpha_L$ versus β_L/α_L defines α_S as the intercept at $\beta_L/\alpha_L = 0$ and β_S as a slope.[1, 3] A determinant method for simultaneous solutions of Eq. (6) has also been described which provides computed average values of γ_{SV}^d, γ_{SV}^p and γ_{SV} in conjunction with the respective standard deviations $\pm\delta^d$, $\pm\delta^p$, and $\pm\delta$.[13] The graphical method via Eq. (7) and the computational method via Eq. (6) are complementary and both will be exploited in this discussion.

RESULTS AND DISCUSSION

Measured values of advancing contact angle, reported as $\cos\theta$, for eleven test liquids (see Table I) upon the fourteen treated fiber or film surfaces included in this study are compiled in Table III. Table IV summarizes the results of surface energy analysis for liquid–solid interactions, where $\cos\theta < 1.00$ (see Table III), using the determinant method. Table V summarizes

TABLE I

Surface tension properties of test liquids at 20°C

Test liquid	γ_{LV}	γ_{LV}^d dyn/cm	γ_{LV}^p	$2\alpha_L$ (dyn/cm)$^{\frac{1}{2}}$	β_L/α_L
Water	72.8	21.8	51.0	9.34	1.53
Glycerol	64.0	34.0	30.0	11.66	0.94
Formamide	58.3	32.3	26.0	11.37	0.90
Ethylene glycol	48.3	29.3	19.0	10.83	0.81
1-Bromonapthalene	44.6	44.6	0.0	13.36	0.00
Glycol PG–E–200	43.5	28.2	15.3	10.62	0.74
Tricresyl phosphate	40.9	39.2	1.7	12.52	0.21
Glycol PG–15–200	36.6	26.0	10.6	10.20	0.64
n-Hexadecane	27.6	27.6	0.0	10.51	0.00
Ethanol (abs.)	22.4	17.0	5.4	8.24	0.56
Hexane	18.4	18.4	0.0	8.58	0.00

the circular equivalent fiber diameter $d \simeq C/\pi = \Delta M \cdot g/\gamma_{LV}\pi$ calculated by Eq. (1) from measured values of ΔM for wetting liquids, where $\cos\theta = 1.00$ (see Table III). The design of the wettability experiment is based upon the application of a series of liquids whose γ_{LV}^p values do not vary systematically with γ_{LV} as shown by Table I. Additionally the liquids should range from nonpolar (saturated hydrocarbons) to highly polar (formamide, glycerol,

TABLE II

Symbols and nomenclature

γ_{LV} = liquid–vapor surface tension
γ_{SV} = solid–vapor surface tension
γ_{S° = surface tension of virgin solid surface in vacuum
π_e = surface free energy reduction due to immersion in ambient vapor phase
α_L, β_L = square root of respective (London-d) dispersion γ_{LV}^d and (Keesom-p) polar parts of γ_{LV}
α_S, β_S = square root of respective dispersion and polar parts of γ_{SV}
W_a = nominal work of adhesion
θ = advancing liquid–solid contact angle

water) in order to provide the broad spectrum of β_L/α_L values. Zisman and coworkers,[15] have shown that a homologous series of liquids with varied γ_{LV} but essentially constant β_L/α_L values form a nearly linear plot of cos θ versus γ_{LV} which on extrapolation to cos θ = 1.00 identifies the critical surface tension γ_c for wetting of the solid surface. This method of representing

TABLE III

Advancing contact angles on treated fiber and film surfaces reported as cos θ

Liquid surface tension γ_{LV} (dyn/cm)	72.8	64.0	58.3	48.3	44.6	43.5	40.9	36.6	27.6	22.4	18.4
						cos θ					
Aluminum coated HT-S ®	0.384	1.00	0.730	1.00	0.963	0.971	0.975	—	0.979	—	1.00
Aluminum coated HM-S ®	0.345	0.955	0.687	0.977	0.932	1.00	1.00	—	0.943	—	0.975
Aluminum coated Thornel 400 ®	0.275	0.978	0.587	0.972	0.946	1.00	0.970	—	0.944	—	1.00
Copper coated Thornel 400 ® (1.5×10^{-5} inch coating)	0.561	0.935	0.732	0.937	0.932	1.00	0.919	—	0.819	0.971	0.956
Copper coated Thornel 400 ® (3.0×10^{-5} inch coating)	0.487	0.929	0.770	0.958	0.967	1.00	0.901	—	0.815	1.00	1.00
Nickel coated HT-S ® (Rockwell treatment 1)	0.465	0.872	0.664	0.893	0.959	—	0.964	0.983	0.971	—	1.00
Nickel coated HT-S ® (Rockwell treatment 2)	0.159	1.00	0.659	0.902	—	—	0.893	—	0.896	—	0.917
Nickel coated HT-S ® (Rockwell treatment 3)	0.367	—	0.539	0.956	—	—	0.954	—	0.966	—	1.0
Nickel coated HT-S ® (Shipley treatment)	0.115	0.643	0.569	0.764	0.950	0.946	0.969	1.00	1.00	—	1.00
Hydrogen treated HT-S ®	0.332	0.954	0.577	0.943	0.970	—	0.994	1.00	0.980	—	1.00
Vacuum heat treated HT-S ®	0.396	0.810	0.670	0.884	0.996	—	0.982	0.992	—	—	1.00
Hexachlorobutadiene polymer coated Thornel 400	0.308	0.536	0.547	0.875	0.939	—	0.958	0.954	—	—	1.00
Hexachlorobutadiene polymer film	0.00	0.326	0.342	0.559	0.990	—	0.988	0.951	—	—	—
Polychloral film	0.00	0.259	0.242	0.682	0.996	—	0.891	0.914	—	—	—

wettability data from Table III is illustrated in the upper views of Figure 5 through Figure 11 for selected surfaces characterized by this study. The lower views of Figure 5 through Figure 11 show the wettability data of Table III in the format defined by Eq. (7) as plots of $W_a/2\alpha_L$ versus β_L/α_L. The solid curves in the lower portion of Figure 5 through Figure 11 are based upon the average values of $\alpha_S = (\gamma_{SV}^d)^{\frac{1}{2}}$ and $\beta_S = (\gamma_{SV}^p)^{\frac{1}{2}}$ reported in Table IV from determinant calculations while the bracketing dashed curves identify the standard deviations $\pm\delta^d$ and $\pm\delta^p$.

In general, one notes a broad scatter of cos θ versus γ_{LV} data in Figure 6 through Figure 8 where the surface energy analysis (see Table IV) resolves a $\gamma_{SV}^p \geqslant 12.5$ dyn/cm for the solid surface. When the polar component of solid

TABLE IV

Calculated dispersion and polar surface energy components of treated graphite fibers using the determinant method [for method see Ref. 13]

	$\gamma_{SV} \pm \delta^d$	$\gamma_{SV}^p \pm \delta^p$	$\gamma_{SV} \pm \delta$
Virgin fibers			
1. Hercules HT-S ® (Ref. 1, 3)	25.9 ± 1.5	25.7 ± 3.3	51.6 ± 2.3
2. Hercules HM-S ® (Ref. 1, 3)	26.1 ± 2.1	26.8 ± 4.1	52.8 ± 2.7
3. Union Carbide Thornel 400 (Ref. 14)	25.5 ± 2.6	23.4 ± 3.6	49.0 ± 1.8
Metallized fibers			
4. Aluminum coated HT-S ®	34.4 ± 1.9	10.7 ± 1.1	45.1 ± 1.0
5. Aluminum coated HM-S ®	36.8 ± 6.8	17.5 ± 4.2	54.2 ± 5.5
6. Aluminum coated Thornel 400 ®	42.7 ± 8.1	13.1 ± 2.9	55.8 ± 7.4
7. Copper coated Thornel 400 (1.5×10^{-5} inch coating)	27.9 ± 2.9	22.0 ± 2.8	49.9 ± 2.1
8. Copper coated Thornel 400 (3.0×10^{-5} inch coating)	34.4 ± 3.9	18.1 ± 2.5	52.5 ± 2.7
9. Nickel coated HT-S ® (Rockwell Treatment 1)	33.9 ± 2.8	13.4 ± 1.9	47.3 ± 2.1
10. Nickel coated HT-S ® (Rockwell Treatment 2)	30.8 ± 4.8	12.5 ± 2.8	43.3 ± 3.2
11. Nickel coated HT-S ® (Rockwell Treatment 3)	28.4 ± 2.1	11.5 ± 1.5	39.9 ± 1.1
12. Nickel coated HT-S ® (Shipley Treatment)	44.9 ± 3.9	4.1 ± 0.9	49.1 ± 3.4
Heat treated fibers			
13. Hydrogen treated HT-S ®	41.1 ± 6.7	12.5 ± 2.7	53.7 ± 6.0
14. Vacuum heat treated HT-S ®	38.2 ± 3.1	9.5 ± 1.6	47.7 ± 2.4
Polymer coated fibers and films			
15. Polyhexachlorobutadiene coated Thornel 400 ®	35.6 ± 1.8	6.7 ± 1.0	42.3 ± 1.1
16. Polyhexachlorobutadiene film	40.7 ± 1.8	0.8 ± 0.2	41.5 ± 0.8
17. Polychloral film	36.6 ± 1.7	1.4 ± 0.3	37.9 ± 1.4

surface tension is of lower magnitude, $\gamma_{SV}^{p} \leqslant 10.0$ dyn/cm, as is the case for Figure 9 through Figure 11 the cos θ versus γ_{LV} data tend to form a narrow rectilinear band as required to resolve a characteristic value of critical surface tension γ_c.

TABLE V

Equivalent diameter $d = C/\pi$ for untreated and treated graphite fibers as determined by Eq. (1) for cos $\theta = 1.00$

	d (μm)
Virgin fibers	
1. Hercules HT-S ® (Ref. 1, 3)	9.96 (see Figure 1)
2. Hercules HM-S ® (Ref. 1, 3)	8.87
3. Union Carbide Thornel 400 ® (Ref. 14)	8.44
Metallized fibers	
4. Al coated HT-S	9.17
5. Al coated HM-S	10.1
6. Al coated Thornel 400	8.59 (see Figures 2 and 6)
7. Cu coated Thornel 400 ($1.5 \cdot 10^{-5}$ inch)	8.56
8. Cu coated Thornel 400 ($3.0 \cdot 10^{-5}$ inch)	8.99 (see Figures 3 and 7)
9. Ni coated HT-S (Rockwell #1)	8.39
10. Ni coated HT-S (Rockwell #2)	7.95 (see Figures 4 and 8)
11. Ni coated HT-S (Rockwell #3)	9.84
12. Ni coated HT-S (Shipley treated)	12.6 (see Figures 5 and 9)
Heat treated fibers	
13. Hydrogen treated HT-S	7.55
14. Vacuum heat treated HT-S	8.55 (see Figure 10)
Polymer coated fiber	
15. Polyhexachlorobutadiene Thornel 400	8.28 (see Figure 11)

The two parameter model for liquid–solid interactions (see Eq. (6) and Eq. (7)) which form the data displays in the lower portions of Figure 6 through Figure 11 provide more detail concerning the origin of data scatter. For example, in Figure 6 the high cos θ and W_a value for glycerol with $\beta_L/\alpha_L = 0.94$ is the principal source for the uncertainty $\delta^d = \pm 8.1$ reported for Al coated Thornel 400 in Table IV. In Figure 8 for Cu (thickness = $3.0 \cdot 10^{-5}$ inch) coated Thornel 400, it is evident that both water with $\beta_L/\alpha_L = 1.53$ and hexadecane with $\beta_L/\alpha_L = 0.0$ fail to linearize well on a plot of $W_a/2\alpha_L$ versus β_L/α_L. The high roughness for this Cu coated graphite fiber shown by Figure 3 may be an important source for the discrepancies in the $W_a/2\alpha_L$ versus β_L/α_L data of Figure 8. With the above noted exceptions, one notes in Figure 7 and Figure 9 through Figure 11 a reasonable linearization of

$W_a/2\alpha_L$ versus β_L/α_L data and corresponding resolution of γ^d_{LV} and γ^p_{LV} values as reported by Table IV. It is thus evident that Eq. (6) or Eq. (7) are capable of resolving discrete exceptions to idealized dispersion–polar interactions. As shown by Table IV surface treatments can provide significant reductions of the high γ^p_{SV} values characteristic of commercial graphite fibers. The data of Table IV also shows a compensating increase in γ^d_{SV} so that the total surface energy γ_{SV} is not substantially diminished by the fiber surface treatment.

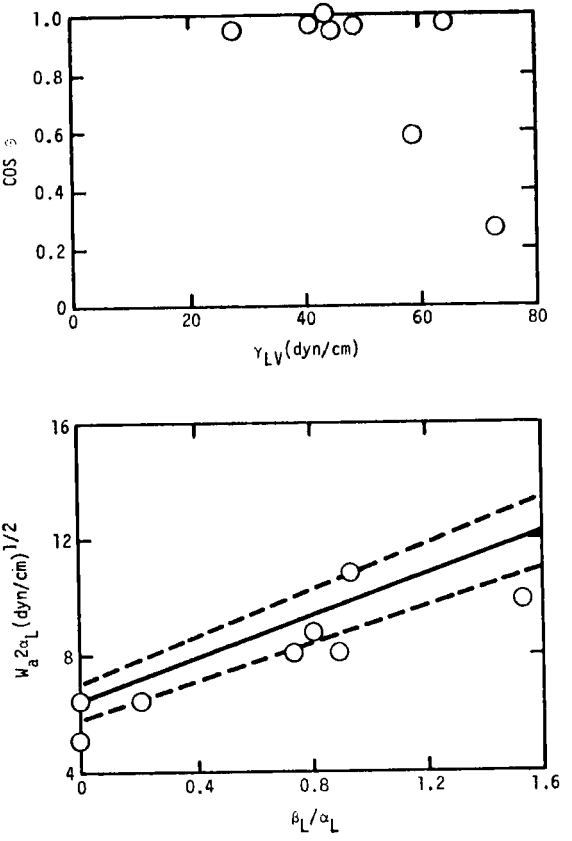

FIGURE 6 Critical surface tension plot (upper view) and $W_a/2\alpha_L$ versus β_L/α_L for Al coated Thornel 400 fiber (see Figure 2 for topology).

The micro-Wilhelmy plate experiment also appears capable of resolving changes in fiber circumference produced by surface treatment. The substantially increased equivalent diameter $d = 12.6\ \mu m$ deduced from wettability measurements in Table V for Ni coated HT–S (Shipley treated) is

confirmed by SEM examination as shown in Figure 5 (i.e. $\simeq 15\ \mu m$). The SEM views of Figure 2 through Figure 4 indicate relatively thin metal coatings and this result is confirmed by the equivalent diameters $d \leqslant 10.0\ \mu m$ reported for these fibers in Table V.

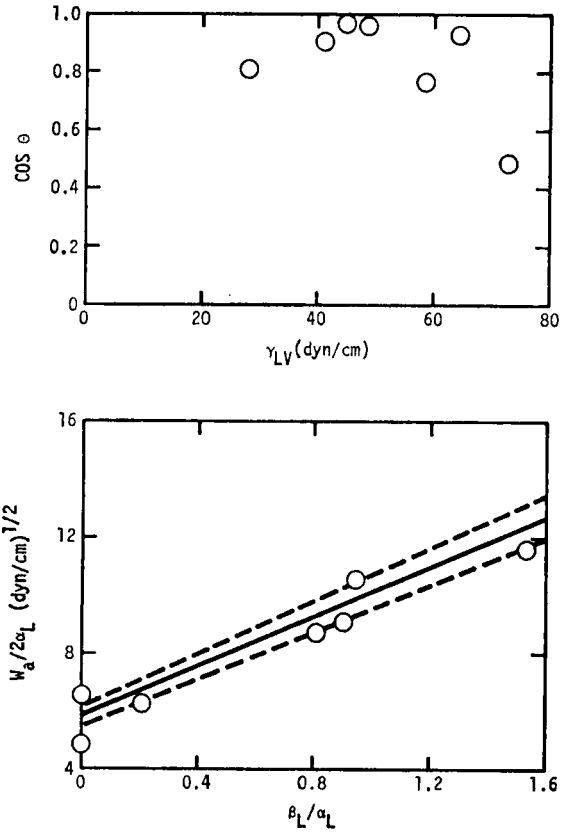

FIGURE 7 Critical surface tension plot (upper view) and $W_a/2\alpha_L$ versus β_L/α_L for Cu coated Thornel 400 fiber (see Figure 3 for topology).

The first objective in modifying the surface properties of reinforcing fibers so as to reduce γ_{SV}^p while holding $\gamma_{SV} = \gamma_{SV}^d + \gamma_{SV}^p$ essentially constant relates to the necessity to retain fiber wettability by the polymer matrix under ambient air immersion. The second objective relates to decreasing the moisture sensitivity of the bonded fiber-matrix interface. The theoretical balance which is struck between these two objectives can be rationalized in terms of the reversible Griffith fracture energy γ_G which is redefined by the

following statement for three phase interactions:[3]

$$\gamma_G = R^2 - R_0^2 \tag{8}$$

$$R_0^2 = 0.25[(\alpha_1 - \alpha_3)^2 + (\beta_1 - \beta_3)^2] \tag{9}$$

$$R^2 = [\alpha_2 - 0.5(\alpha_1 + \alpha_3)]^2 + [\beta_2 - 0.5(\beta_1 + \beta_3)]^2 \tag{10}$$

where α_1, β_1 = matrix surface properties, α_2, β_2 = surface properties of immersion phase at the crack tip, and α_3, β_3 = fiber surface properties as defined by symbols of Table II for liquid and solid surfaces.

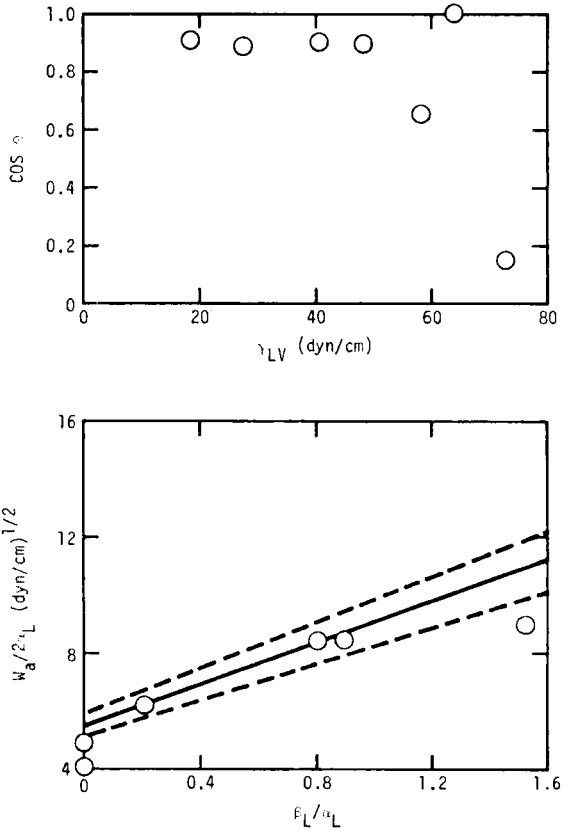

FIGURE 8 Critical surface tension plot (upper view) and $W_a/2\alpha_L$ versus β_L/α_L for Ni coated HT-S fiber (see Figure 4 for topology).

The standard Griffith–Irwin relation in fracture mechanics defines the critical stress intensity factor K_{1c} by the following statement:[16, 17]

$$K_{1c} \approx [2E(\gamma_G + W_p)]^{\frac{1}{2}} \tag{11}$$

where E = Young's modulus, W_p = plastic work associated with crack extension, and γ_G is defined by Eq. (8). Recent studies have shown that $W_p \propto \gamma_G^4$ thereby indicating that K_{1c} which is a direct measure of fracture toughness is very sensitive to environmental (phase 2) effects upon γ_G.[3, 4] As shown by Eq. (8), the Griffith surface energy γ_G is increased by reducing

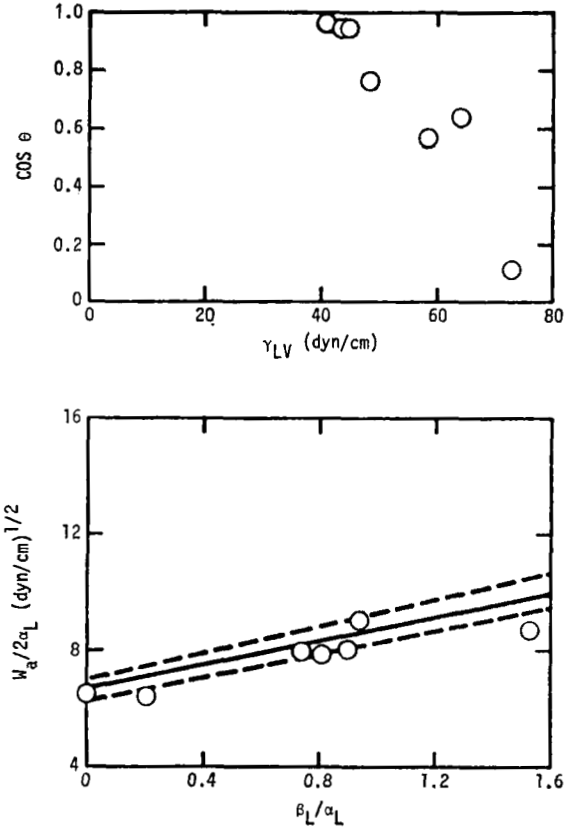

FIGURE 9 Critical surface tension plot (upper view) and $W_a/2\alpha_L$ versus β_L/α_L for Ni (Shipley) coated HT-S fiber (see Figure 5 for topology).

R_0 and increasing R. The reduction of R_0 is shown by Eq. (9) to involve the close matching of the surface properties of matrix (phase 1) and fiber (phase 3) so that $\alpha_1 \simeq \alpha_3$ and $\beta_1 \simeq \beta_3$ in which case $R_0 \simeq 0$. By assuming the optimum resin/matrix interface displays $R_0 \simeq 0$ it follows that increasing $\alpha_3 = (\gamma_{SV}^d)^{\frac{1}{2}}$ and decreasing $\beta_3 = (\gamma_{SV}^p)^{\frac{1}{2}}$ for the fiber surface permits selection of matrix materials with corresponding high $\alpha_1 \simeq \alpha_3$ and low $\beta_1 \simeq \beta_3$ values.

The average values of γ_{SV}^d and γ_{SV}^p for virgin fibers and surface treated

fibers and films listed in Table IV are presented as numbered points on the diagram of α versus β shown in Figure 12. Also included in Figure 12 are the surface tension properties of air, with $\alpha_2 = \beta_2 = 0$, and water with $\alpha_2 = 4.67$ $(\text{dyn/cm})^{\frac{1}{2}}$ and $\beta_2 = 7.14$ $(\text{dyn/cm})^{\frac{1}{2}}$ as significant immersion phases.

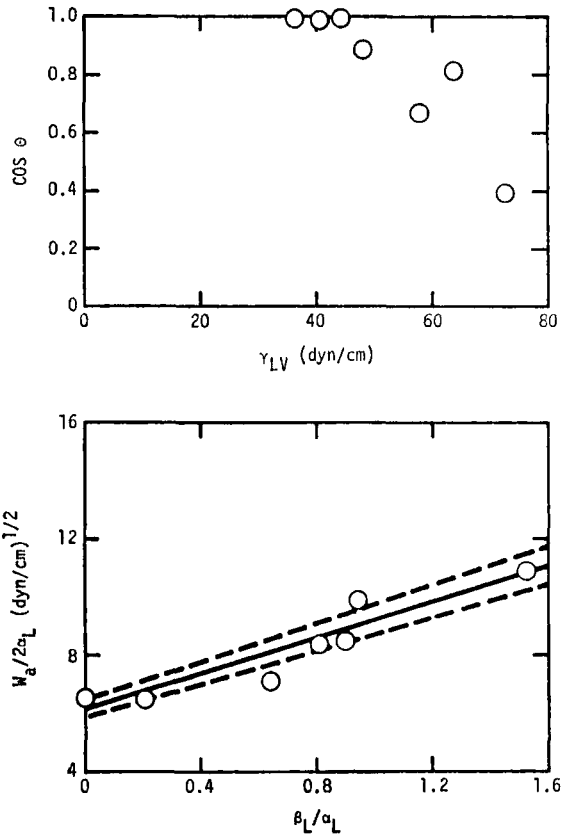

FIGURE 10 Critical surface tension plot (upper view) and $W_a/2\alpha_L$ versus β_L/α_L for vacuum heat treated HT-S fiber.

It is evident in Figure 12 that untreated fibers with $\alpha_3 \simeq \beta_3 \simeq 5.0$ dyn/cm (solids 1, 2 and 3 of Table IV) require matrix materials of equivalent high polar character $\alpha_1 \simeq \beta_1 \simeq 5.0$ dyn/cm to provide $R_0 \simeq 0$. As indicated by the data points of Figure 12, the metallized graphite fibers (solids 4–12 of Table IV) display a range of α_3, β_3 values which are shifted toward increased dispersion α and decreased polar β character with Ni coated HT-S (Shipley treatment) as the least polar. Thermal treatments (solids 13 and 14 of Table IV) provide significant increases in α_3 and β_3 as compared to the majority

of metallizing treatments. Coatings of highly chlorinated polymers (solids 15–17 of Table IV) display a high efficiency in increasing α_3 and reducing β_3 as compared to both metallizing and thermal treatments of graphite fibers.

For the preferred case where $R \simeq 0$ with $\alpha_1 \simeq \alpha_3$ and $\beta_1 \simeq \beta_1$ in Eq. (9), it follows that Eq. (8) can be restated as follows:

$$\gamma_G^{\frac{1}{2}} = R = [(\alpha_2 - \alpha_3)^2 + (\beta_2 - \beta_3)^2]^{\frac{1}{2}} \qquad [R_0 = 0]. \tag{12}$$

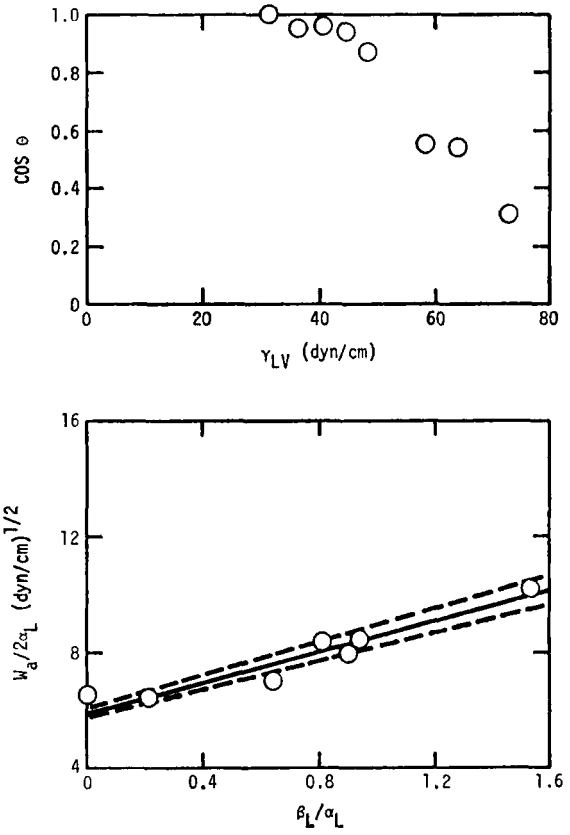

FIGURE 11 Critical surface tension plot (upper view) and $W_a/2\alpha_L$ versus β_L/α_L for polyhexachlorobutadiene coated Thornel 400 fiber.

The dual requirement of maintaining a high γ_G in both air and water immersion can be graphically represented on the dispersion α versus polar β surface energy diagram of Figure 12. For commercially treated HT-S graphite fiber (surface 1 of Table IV) Figure 12 shows $R(H_2O) = 7.18$ $(dyn/cm)^{\frac{1}{2}}$ and $R(air) = 2.06$ $(dyn/cm)^{\frac{1}{2}}$ as calculated from Eq. (12). The ratio of $\gamma_G^{\frac{1}{2}}(H_2O)/\gamma_G^{\frac{1}{2}}(air) = 0.272$ predicts a high moisture sensitivity for the

$R_0 = 0$ matrix/fiber interface. This prediction has been confirmed by experimental studies[3] of an epoxy/graphite fiber composite with interface properties closely matching the case shown in Figure 12. By shifting the fiber and matrix surface properties so that $\alpha_1 \simeq \alpha_3 \geqslant 6.0\,(\text{dyn/cm})^{\frac{1}{2}}$ and $\beta_1 \simeq \beta_3 \leqslant 1.5\,(\text{dyn/cm})^{\frac{1}{2}}$ as indicated by the shaded region in Figure 12, it follows from Eq. (12) the high dispersion and low polar character of the bonded fiber/matrix interface should provide an optimized strong interfacial bonding and low moisture sensitivity.

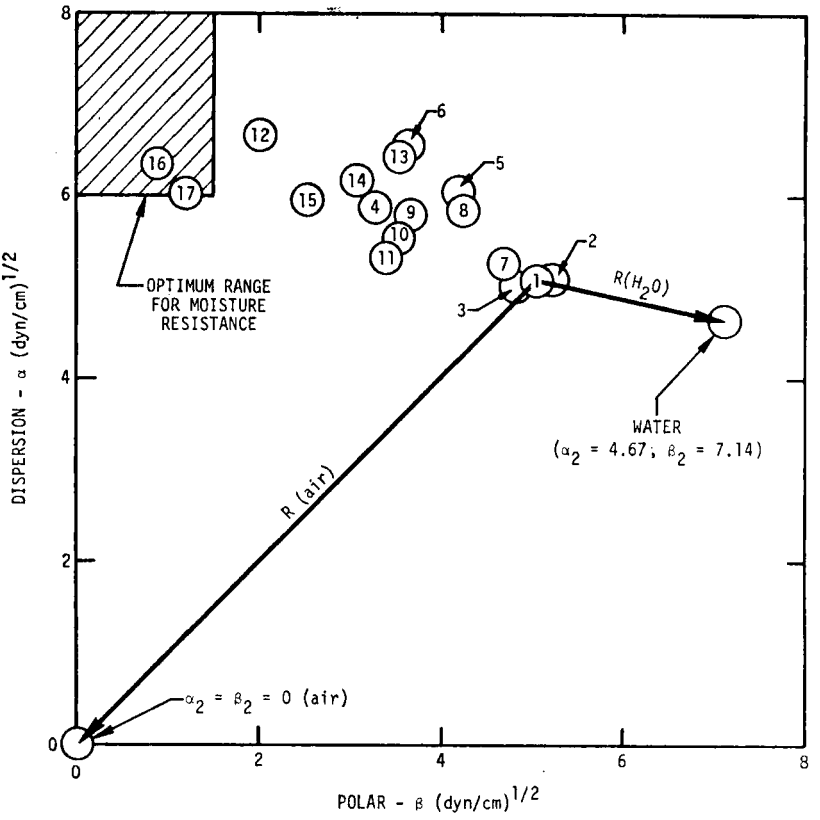

FIGURE 12 Dispersion energy component α versus polar component β for surface properties of fibers (see Table IV) with zone of optimum zone for moisture resistance indicated by shaded area.

SUMMARY AND CONCLUSIONS

This study shows that several types of surface treatment for commercial graphite fibers produce increased dispersion $\gamma_{SV}^{d} = \alpha_3^2$ and reduced polar

$\gamma_{SV}^p = \beta_3^2$ contributions to the fiber surface tension $\gamma_{SV} = \alpha_3^2 + \beta_3^2$ properties. The most effective surface treatments for achieving high $\alpha_3 \geqslant 6.0$ (dyn/cm)$^{\frac{1}{2}}$ and low $\beta_3 \leqslant 1.5$ (dyn/cm) appear from this study to involve polymer coatings of either polyhexachlorobutadiene or polychloral (solids 16 and 17 of Table IV). These highly chlorinated polymers provide the requisite balance of Griffith fracture energies:

$$\gamma_G(\text{air}) \simeq \gamma_G(H_2O) = (R^2 R_0^2) \geqslant 36 \text{ dyn/cm}$$

defined by the shaded region of Figure 12 when matrix and resin surface properties are matched so that $R_0 \simeq 0$, yet retaining spontaneous spreading of the matrix on the fiber during the process of impregnation.[3]

Thermal treatments of graphite fiber intended to reduce polar surface functionality are indicated in this study to be less effective than polymer coatings. Metallizing with Al, Cu, and Ni produce a varied range of fiber topologies and surface properties. Examination of literature data[13] for other polymers with high γ_{SV}^d and low γ_{SV}^p shows that nonpolar aromatic polymers such as polyethyleneterepthalate $\alpha_3 = 6.05$, $\beta_3 = 1.70$ (dyn/cm)$^{\frac{1}{2}}$ and polystyrene $\alpha_3 = 6.20$, $\beta_3 = 1.65$ (dyn/cm)$^{\frac{1}{2}}$ and chlorocarbons such as polyvinyl chloride $\alpha_3 = 6.17$, $\beta_3 = 1.87$ (dyn/cm)$^{\frac{1}{2}}$ and polyvinylidene chloride $\alpha_3 = 6.18$, $\beta_3 = 1.78$ (dyn/cm)$^{\frac{1}{2}}$ display surface properties which correlate with the optimum response region of Figure 12. To serve as an effective fiber coating material for surface energy modification, it is evident that the coating must be thermally stable, highly crosslinked, and preferably chemically grafted to the fiber surface.

The reduction of polar character in fiber and matrix surface properties provides a corresponding reduction in bulk polar character in terms of the solubility properties of the matrix phase.[13] This reduction in bulk polar character would be expected to diminish the effects of moisture upon the rheological response of polymer matrix composites.

Acknowledgement

The authors wish to thank Dr. H. C. Miller, du Pont Company for polychloral samples and Dr. J. R. Lewis, Rocketdyne Division, Rockwell International, for copper plated graphite fibers. This work was supported in part by the Rockwell International IR & D Interdivisional Technology Program under the sponsorship of the Composites Technical Panel.

References

1. D. H. Kaelble, *Proc. 23rd Int. Cong. of Pure and Appl. Chem.* **8** (Butterworth, London, 1971). Pp. 265–302.
2. D. H. Kaelble, *J. Adhesion* **5**, 245 (1973).
3. D. H. Kaelble, P. J. Dynes, and E. H. Cirlin, *J. Adhesion* **5**, in press (1973).
4. B. Harris, P. W. R. Beaumont, and E. M. de Ferran, *J. Matl. Sci.* **6**, 238 (1971).

5. U.S. Patent No. 3,462,288, August 19, 1969.
6. J. R. Lewis, "Copper/Graphite Composites," Interdivisional Technology Program Report, Nov. 1971, Rocketdyne Division, Rockwell International Corp.
7. A. N. Wright, *Nature* **215**, 953 (1967).
8. C. O. Kunz, P. C. Long, and A. N. Wright, *Polymer Eng. and Sci.* **12**, 209 (1967).
9. A. W. Neumann and W. Tanner, *Proc. 5th Int. Cong. on Surface Activity* **2** (1968). Pp. 727–734.
10. G. Mozzo and R. Chabord, *Proc. 23rd Annual Conf. Reinforced Plastics/Composites Division*, Soc. Plastics Industry, Section 9–C (1968). Pp. 1–8.
11. F. M. Fowkes, in *Treatise on Adhesion and Adhesives*, Ed. R. L. Patrick, Vol. 1, Chap. 9 (Dekker, New York, 1967).
12. J. R. Dann. *J. Colloid Interface Sci.* **32**, 321 (1970).
13. D. H. Kaelble, *Physical Chemistry of Adhesion*, Chap. 4–5 (Wiley, New York, 1971).
14. P. J. Dynes and D. H. Kaelble, *J. Adhesion*, in press.
15. W. A. Zisman, in *Adhesion and Cohesion*, Ed. P. Weiss (Elsevier, Amsterdam, 1962). P. 176.
16. G. R. Irwin, "Fracture Mechanics," in *Structural Mechanics* (Pergamon Press, New York, 1960). Pp. 557–594.
17. G. R. Irwin, in *Treatise on Adhesion and Adhesives*, Ed. R. L. Patrick (Dekker, New York, 1972). Pp. 233–267.